Markovian Modelling of Internet Traffic

António Nogueira[1], Paulo Salvador[1], Rui Valadas[2], and António Pacheco[3]

[1] University of Aveiro / Institute of Telecommunications Aveiro
Campus de Santiago, 3810-193 Aveiro, Portugal
{nogueira,salvador}@ua.pt
[2] Instituto Superior Técnico - UTL
Department of Electrical and Computing Engineering
Av. Rovisco Pais, 1049-001 Lisboa, Portugal
{rui.valadas}@ist.utl.pt
[3] Instituto Superior Técnico - UTL
Department of Mathematics and CEMAT
Av. Rovisco Pais, 1049-001 Lisboa, Portugal
{apacheco}@math.ist.utl.pt

Abstract. This tutorial discusses the suitability of Markovian models to describe IP network traffic that exhibits peculiar scale invariance properties, such as self-similarity and long range dependence. Three Markov Modulated Poisson Processes (MMPP), and their associated parameter fitting procedures, are proposed to describe the packet arrival process by incorporating these peculiar behaviors in their mathematical structure and parameter inference procedures. Since an accurate modeling of certain types of IP traffic requires matching closely not only the packet arrival process but also the packet size distribution, we also discuss a discrete-time batch Markovian arrival process that jointly characterizes the packet arrival process and the packet size distribution. The accuracy of the fitting procedures is evaluated by comparing the long range dependence properties, the probability mass function at each time scale and the queuing behavior corresponding to measured and synthetic traces generated from the inferred models.

Keywords: Long range dependence, self-similarity, time scale, Markov Modulated Poisson Process, packet arrival (size) process.

1 Introduction

The growing diversity of services and applications for IP networks has been driving a strong requirement to make frequent measurements of packet flows and to describe them through appropriate traffic models. Several studies have already shown that IP traffic may exhibit properties of self-similarity and/or long-range dependence (LRD) [1, 2, 3, 4, 5], peculiar behaviors that have a significant impact on network performance. However, matching LRD is only required within the time-scales of interest to the system under study [6, 7]: for example, in order to analyze queuing behavior the selected traffic model only needs to capture the correlation structure of the source up to the so-called critical time-scale or correlation horizon, which is directly related to the maximum

D. Kouvatsos (Ed.): Next Generation Internet, LNCS 5233, pp. 98–124, 2011.

buffer size [5,8,9]. One of the consequences of this result is that more traditional traffic models such as Markov Modulated Poisson Processes (MMPPs) can still be used to model traffic exhibiting LRD [10, 11, 12, 13]. However, providing a good match of the LRD characteristics through an accurate fitting of the autocovariance tail is not enough for accurate prediction of the queuing behavior [14]. In general, an accurate prediction of the queuing behavior requires detailed modeling of the first-order statistics, not just the mean, and for certain types of network traffic it demands the incorporation of time-dependent scaling laws [15, 16, 17].

This tutorial discusses the suitability of Markovian models, based on MMPPs, for modeling IP traffic. Traffic modeling is usually concerned with the packet arrival process, aiming to fit its main characteristics. In order to describe the packet arrival process, we will present three traffic models that were designed to capture self-similar behavior over multiple time scales. The first model is based on a parameter fitting procedure that matches both the autocovariance and marginal distribution of the counting process [18]. The MMPP is constructed as a superposition of L two-state MMPPs (2-MMPPs), designed to match the autocovariance function, and one M-MMPP designed to match the marginal distribution. Each 2-MMPP models a specific time scale of the data. The second model is a superposition of MMPPs, where each MMPP describes a different time scale [19,20]. The third model is obtained as the equivalent to an hierarchical construction process that, starting at the coarsest time scale, successively decomposes MMPP states into new MMPPs to incorporate the characteristics offered by finner time scales [21]. Both models are constructed by fitting the distribution of packet counts in a given number of time scales. For all three traffic models, the number of states is not fixed *a priori* but is determined as part of the inference procedure. The accuracy of the different models will be evaluated by comparing the probability mass function (PMF) at each time scale, as well as the packet loss ratio (PLR) corresponding to measured traces (exhibiting LRD and self-similar behavior) and traces synthesized according to the proposed models.

It is known that the accurate modeling of certain types of IP traffic requires matching closely not only the packet arrival process but also the packet size distribution [22, 23]. In this way, we also present a discrete-time batch Markovian arrival process (dBMAP) [24, 25, 26] that jointly characterizes the packet arrival process and the packet size distribution, while achieving accurate prediction of queuing behavior for IP traffic exhibiting LRD behavior. In this dBMAP, packet arrivals occur according to a dMMPP and each arrival is further characterized by a packet size with a general distribution that may depend on the phase of the dMMPP. This allows having a packet size distribution closely related to the packet arrival process, which is in contrast with other approaches [22, 23] where the packet size distribution is fitted prior to the matching of the packet arrival rates.

2 Notions of Self-similarity and Long-Range Dependence

Consider the continuous-time process $Y(t)$ representing the traffic volume (e.g. in bytes) from time 0 up to time t and let $X(t) = Y(t) - Y(t-1)$ be the corresponding increment process (e.g. in bytes/second). Consider also the sequence $X^{(m)}(k)$ that is obtained by averaging $X(t)$ over non-overlapping blocks of length m, that is

$$X^{(m)}(k) = \frac{1}{m}\sum_{i=1}^{m} X((k-1)m+i), k = 1, 2, ... \quad (1)$$

The fitting procedure that are presented in this work are based on the aggregated processes $X^{(m)}(k)$.

$Y(t)$ is exactly self-similar when it is equivalent, in the sense of finite-dimensional distributions, to $a^{-H}Y(at)$, for all $t > 0$ and $a > 0$, where H $(0 < H < 1)$ is the Hurst parameter. Clearly, the process $Y(t)$ can not be stationary. However, if $Y(t)$ has stationary increments then again $X(k) = X^{(1)}(k)$ is equivalent, in the sense of finite-dimensional distributions, to $m^{1-H}X^{(m)}(k)$. This illustrates that a traffic model developed for fitting self-similar behavior must preferably enable the matching of the distribution on several time scales.

Long-range dependence is associated with stationary processes. Consider now that $X(k)$ is second-order stationary with variance σ^2 and autocorrelation function $r(k)$. Note that, in this case, $X^{(m)}(k)$ is also second-order stationary. The process $X(k)$ has long-range dependence (LRD) if its autocorrelation function is non-summable, that is, $\sum_n r(n) = \infty$. Intuitively, this means that the process exhibits similar fluctuations over a wide range of time scales. Taking for instance the October Bellcore trace, that is publicly available [1], it can be seen from Figure 1 that the fluctuations over the 0.01, 0.1 and 1s time scales are indeed similar.

Equivalently, one can say that a stationary process is LRD if its spectrum diverges at the origin, that is $f(v) \sim c_f|v|^{-\alpha}, v \to 0$. Here, α is a dimensionless scaling exponent, that takes values in $(0, 1)$; c_f takes positive real values and has dimensions of variance. On the other hand, a short range dependent (SRD) process is simply a stationary process which is not LRD. Such a process has $\alpha = 0$ at large scales, corresponding to white noise at scales beyond the so-called characteristic scale or correlation horizon. The Hurst parameter H is related with α by $H = (\alpha + 1)/2$.

There are several estimators of LRD. In this paper we use the semi-parametric estimator developed in [27], which is based on wavelets. Here, one looks for alignment in the so-called Logscale Diagram (LD), which is a log-log plot of the variance estimates (y_j) of the discrete wavelet transform coefficients representing the traffic

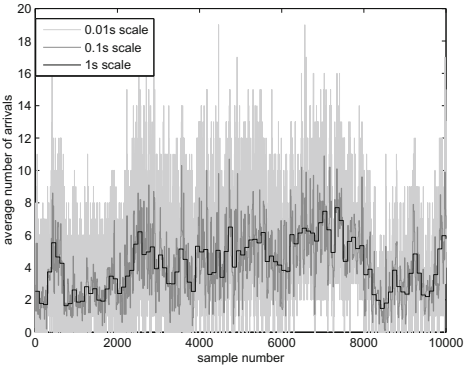

Fig. 1. LRD processes exhibit fluctuations over a wide range of time scales (Example: trace pOct)

process, against scale (j), completed with confidence intervals about these estimates at each scale. It can be thought of as a spectral estimator where large scale corresponds to low frequency. The main properties explored in this estimator are the stationarity and short-term correlations exhibited by the process of discrete wavelet transform coefficients and the power-law dependence in scale of the variance of this process. Traffic is said to be LRD if, within the limits of the confidence intervals, the log of the variance estimates fall on a straight line, in a range of scales from some initial value j_1 up to the largest one present in data and the slope of the straight line, which is an estimate of the scaling exponent α, lies in $(0, 1)$.

There is a close relationship between long-range dependent and self-similar processes. In fact, if $Y(t)$ is self-similar with stationary increments and finite variance then $X(k)$ is long-range dependent, as long as $\frac{1}{2} < H < 1$. The process $X(k)$ is said to be exactly second-order self-similar ($\frac{1}{2} < H < 1$) if

$$r\,(n) = 1/2\left[(n+1)^{2H} - 2n^{2H} + (n-1)^{2H}\right] \tag{2}$$

for all $n \geq 1$, or is asymptotically self-similar if

$$r\,(n) \sim n^{-(2-2H)} L(n) \tag{3}$$

as $n \to \infty$, where $L(n)$ is a slowly varying function at infinity. In both cases the autocovariance decays hyperbolically, which indicates LRD. Any asymptotically second-order self-similar process is LRD, and vice-versa.

3 Background on Markovian Models

The dBMAP stochastic process may be regarded as an Markov random walk whose additive component takes values on the nonnegative integers, $\mathbb{N}_0$. Thus, we say that a Markov chain $(Y, J) = \{(Y_k, J_k),\, k \in \mathbb{N}_0\}$ on the state space $\mathbb{N}_0 \times S$ is a dBMAP if

$$P(Y_{k+1} = m,\, J_{k+1} = j | Y_k = n,\, J_k = i) = \begin{cases} 0 & m < n \\ p_{ij}\, q_{ij}(m-n) & m \geq n \end{cases} \tag{4}$$

where $\mathbf{P} = (p_{ij})_{i,j\in S}$ is a stochastic matrix and, for each pair $(i, j) \in S^2$, $q_{ij} = \{q_{ij}(n),\, n \in \mathbb{N}_0\}$ is a probability function over $\mathbb{N}_0$, and we let $\mathbf{Q}(n) = (q_{ij}(n))_{i,j\in S}$. This implies, in particular that J is a Markov chain, called the *Markov component* or *phase* of (Y, J) and S is the set of modulating states or the phase set. When the dBMAP (Y, J) is used to model an arrival process, Y_k may be interpreted as the total number of arrivals until instant k. (X, J) is also a dBMAP, where X_n represents the total number of packets that arrive until instant n.

An important particular case of the dBMAP is the dMMPP. We say that the process (Y, J) on the state space $\mathbb{N}_0 \times S$ is a dMMPP with parameters $(\mathbf{P}, \Lambda)$, where $\mathbf{P} = (p_{ij})_{i,j\in S}$ is a stochastic matrix and $\Lambda = (\lambda_{ij})_{i,j\in S} = (\lambda_i 1_{\{i=j\}})_{i,j\in S}$ is a diagonal matrix with nonnegative entries (i.e., $\lambda_i \geq 0$, $i \in S$), if it is a dBMAP with parametrization $(\mathbf{P}, \{\mathbf{Q}(n),\, n \in \mathbb{N}\})$, where

$$q_{ij}(n) = e^{-\lambda_j} \frac{\lambda_j^n}{n!} \tag{5}$$

for $i, j \in S$ and $n \in \mathbb{N}$; i.e., $q_{ij} = \{q_{ij}(n), n \in \mathbb{N}_0\}$ is the probability function of a Poisson random variable with mean λ_j. Thus a dMMPP is a dBMAP for which the number of arrivals in a given instant of time is only a function of the current phase of the dBMAP and when the process is in phase j the number of arrivals at an instant has a Poisson distribution with mean λ_j; the parameter λ_j may be null, in which case no arrivals occur in phase j. So, (Y, J) is a dMMPP with set of modulating states S and parameter (matrices) $\mathbf{P}$ and $\mathbf{\Lambda}$, and write

$$(Y, J) \sim \text{dMMPP}_S(\mathbf{P}, \mathbf{\Lambda}) \tag{6}$$

where $\mathbf{\Lambda} = (\lambda_{ij}) = (\lambda_i \delta_{ij})$. The matrix $\mathbf{P}$ is the transition probability matrix of the modulating Markov chain J, whereas $\mathbf{\Lambda}$ is the matrix of Poisson arrival rates. If S has cardinality r, we say that (Y, J) is a dMMPP of order r (dMMPP$_r$). The stationary distribution of J is denoted by $\pi = [\pi_1\, \pi_2, \ldots\, \pi_r]$.

The superposition of independent dMMPPs is still an dMMPP. More precisely, if $(Y^{(l)}, J^{(l)}) \sim \text{dMMPP}_{r_l}(\mathbf{P}^{(l)}, \Lambda^{(l)})$, $l = 1, 2, \ldots, L$, are independent, then their superposition $(Y, J) = (\sum_{l=1}^{L} Y^{(l)}, (J^{(1)}, J^{(2)}, \ldots, J^{(L)}))$ is a dMMPP$_S(\mathbf{P}, \Lambda)$, where $S = \{1, 2, \ldots, r_1\} \times \ldots \times \{1, 2, \ldots, r_L\}$,

$$\mathbf{P} = \mathbf{P}^{(1)} \otimes \mathbf{P}^{(2)} \otimes \ldots \otimes \mathbf{P}^{(L)} \tag{7}$$

and

$$\Lambda = \Lambda^{(1)} \oplus \Lambda^{(2)} \oplus \ldots \oplus \Lambda^{(L)} \tag{8}$$

with $\oplus$ and $\otimes$ denoting the Kronecker sum and product, respectively.

4 M2^L-MMPP - A Second-Order Self-similar Model

This section describes a parameter fitting procedure, based on MMPPs, that matches both the autocovariance and the marginal distribution of the counting process, leading to accurate estimates of queuing behavior for network traffic exhibiting LRD behavior. This work was firstly published in [18] and was also motivated by the need to keep the number of states of the MMPP at a minimum in order to reduce the complexity associated with the calculation of the performance metrics of interest.

Matching simultaneously the autocovariance and marginal distribution of the counting process is a difficult task since every MMPP parameter influences both characteristics. With the purpose of achieving some degree of decoupling when matching

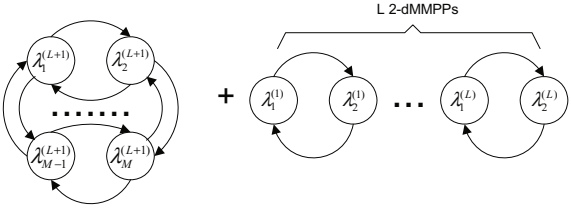

Fig. 2. Superposition of an M-dMMPP and L 2-dMMPP models

these two statistics, the proposed MMPP, $(X, J) \sim \text{M}2^L\text{-dMMPP}$, is constructed as a superposition of L independent 2-dMMPPs, $(X^{(l)}, J^{(l)}) \sim \text{dMMPP}_2(\mathbf{P}^{(l)}, \Lambda^{(l)}), l = 1, 2, \ldots, L$, that capture the autocovariance function of the increments of the arrival process and one M-dMMPP, $(X^{(L+1)}, J^{(L+1)}) \sim \text{dMMPP}_M(\mathbf{P}^{(L+1)}, \Lambda^{(L+1)})$, that approximates the distribution of the increments of the arrival process. This superposition step is graphically illustrated in Figure 2. In this approach L and M are not fixed *a priori* but instead are computed as part of the fitting procedure.

Let us define the increment processes $Y^{(1)}, Y^{(2)}, \ldots, Y^{(L+1)}$ and Y associated to $X^{(1)}, X^{(2)}, \ldots, X^{(L+1)}$, and X, respectively:

$$Y_k^{(l)} = X_{k+1}^{(l)} - X_k^{(l)},\ l = 1, 2, \ldots, L+1 \tag{9}$$

and

$$Y_k = X_{k+1} - X_k \tag{10}$$

for $k = 0, 1, \ldots$. Note that Y_k is the (total) number of arrivals at sampling interval k and $Y_k^{(l)}$ is the number of arrivals that are due to the l-th arrival process, so that, in particular,

$$Y_k = \sum_{l=1}^{L+1} Y_k^{(l)}, \quad k = 0, 1, 2, \ldots. \tag{11}$$

Moreover, $Y^{(1)}, Y^{(2)}, \ldots, Y^{(L+1)}$, and Y, are stationary sequences.

In order to characterize the marginal distributions of the L 2-dMMPPs processes, $Y^{(1)}, Y^{(2)}, \ldots, Y^{(L)}$, the M-dMMPP, $Y^{(L+1)}$, and the resulting process, Y, we denote by $\{f_l(k),\ k = 0, 1, 2, \ldots\}$, $l = 1, 2, \ldots, L+1$, and $\{f(k),\ k = 0, 1, 2, \ldots\}$, their (marginal) probability functions, respectively. As the univariate distributions of $Y^{(1)}$, $Y^{(2)}, \ldots, Y^{(L+1)}$ are mixtures of Poisson distributions, we denote the probability function of a Poisson random variable with mean μ by $\{g_\mu(k),\ k = 0, 1, 2, \ldots\}$, for $\mu \in [0, +\infty)$, so that $g_\mu(k) = e^{-\mu}\, \frac{\mu^k}{k!}$, $k = 0, 1, 2, \ldots$. For $l = 1, 2 \ldots, L$, the marginal distribution of $Y^{(l)}$ (that is, the distribution of $Y_k^{(l)}$, for $k = 0, 1, \ldots$) is a mixture of two Poisson distributions with means $\lambda_1^{(l)}$ and $\lambda_2^{(l)}$ and weights $\pi_1^{(l)}$ and $\pi_2^{(l)}$, respectively. Thus the probability functions of $Y^{(l)}$, $l = 1, 2, \ldots, L$, are given by

$$f_l(k) = \pi_1^{(l)}\, g_{\lambda_1^{(l)}}(k) + \pi_2^{(l)}\, g_{\lambda_2^{(l)}}(k), k = 0, 1, 2, \ldots \tag{12}$$

and their autocovariance functions are

$$\gamma_k^{(l)} = \text{Cov}\,(Y_0^{(l)}, Y_k^{(l)}) = \pi_1^{(l)}\, \pi_2^{(l)}\, |\lambda_2^{(l)} - \lambda_1^{(l)}|^2\, e^{k c_l}, k = 0, 1, 2, \ldots \tag{13}$$

where $c_l = \ln\,(1 - p_{12}^{(l)} - p_{21}^{(l)})$. Note that, in particular, the autocovariance functions of $Y^{(1)}, Y^{(2)}, \ldots, Y^{(L)}$ exhibit an exponential decay to zero.

As we want the M-dMMPP to approximate the distribution of the increments of the arrival process but to have no contribution to the autocovariance function of the increments of the $\text{M}2^L$-dMMPP, we choose to make $J^{(L+1)}$ a Markov chain with no memory whatsoever. This is accomplished by choosing

$$\mathbf{P}^{(L+1)} = \begin{bmatrix} \pi_1^{(L+1)} & \pi_2^{(L+1)} & \dots & \pi_M^{(L+1)} \\ \pi_1^{(L+1)} & \pi_2^{(L+1)} & \dots & \pi_M^{(L+1)} \\ \dots & \dots & \dots & \dots \\ \pi_1^{(L+1)} & \pi_2^{(L+1)} & \dots & \pi_M^{(L+1)} \end{bmatrix} \tag{14}$$

The probability function of $Y^{(L+1)}$ is given by

$$f_{L+1}(k) = \sum_{j=1}^{M} \pi_j^{(L+1)} \, g_{\lambda_j^{(L+1)}}(k), \; k = 0, 1, 2, \dots \tag{15}$$

and the autocovariance function of $Y^{(L+1)}$ is null for all positive lags; i.e.,

$$\gamma_k^{(L+1)} = \text{Cov}\,(Y_0^{(L+1)}, Y_k^{(L+1)}) = 0, \; k \geq 1. \tag{16}$$

Taking into account (11), it follows that the probability function of Y is given by:

$$\begin{aligned} &f(k) = (f_1 * f_2 * \dots * f_{L+1})\,(k) = \\ &= \textstyle\sum_{j_1=1}^{2} \sum_{j_2=1}^{2} \cdots \sum_{j_L=1}^{2} \sum_{j_{L+1}=1}^{M} \left(\prod_{l=1}^{L+1} \pi_{j_l}^{(l)} \right) g_{\sum_{l=1}^{L+1} \lambda_{j_l}^{(l)}}(k) \end{aligned} \tag{17}$$

where * denotes the convolution of probability functions and the autocovariance function is given by

$$\begin{aligned} \gamma_k = \text{Cov}\,(Y_0, Y_k) &= \sum_{l=1}^{L+1} \text{Cov}\left(Y_0^{(l)}, Y_k^{(l)}\right) \\ &= \textstyle\sum_{l=1}^{L} \pi_1^{(l)} \, \pi_2^{(l)} \, |\lambda_2^{(l)} - \lambda_1^{(l)}|^2 \, e^{k c_l}, k = 1, 2, \dots \end{aligned} \tag{18}$$

The inference procedure is illustrated in the flow diagram of Figure 3 and can be divided in four major steps.

A. Approximation of the empirical autocovariance by a weighted sum of exponentials and identification of the time scales

Our approach approximates the autocovariance by a large number of exponentials and then aggregates exponentials with a similar decay into the same time-scale, which is close to the approaches considered in [10, 13, 28] (Figure 4). As a first step, we approximate the empirical autocovariance by a sum of K exponentials with real positive weights and negative real time constants. We chose K as $\sqrt{k_{max}}$, where k_{max} represents the number of points of the empirical autocovariance. This is accomplished through a modified Prony algorithm [29]. The Prony algorithm returns two vectors, $\boldsymbol{a} = [a_1, ..., a_K]$ and $\boldsymbol{b} = [b_1, ..., b_K,]$, which correspond to the approximating function

$$C_K\,(\boldsymbol{a}, \boldsymbol{b}) = \sum_{i=1}^{K} a_i e^{-b_i k}, \quad k = 1, 2, 3, ... \tag{19}$$

At this point we identify the components of the autocovariance that characterize the different time-scales by defining L different time-scales in which the autocovariance decays, $b_i, i = 1, ..., K$, fall in the same logarithmic scale. The components of the

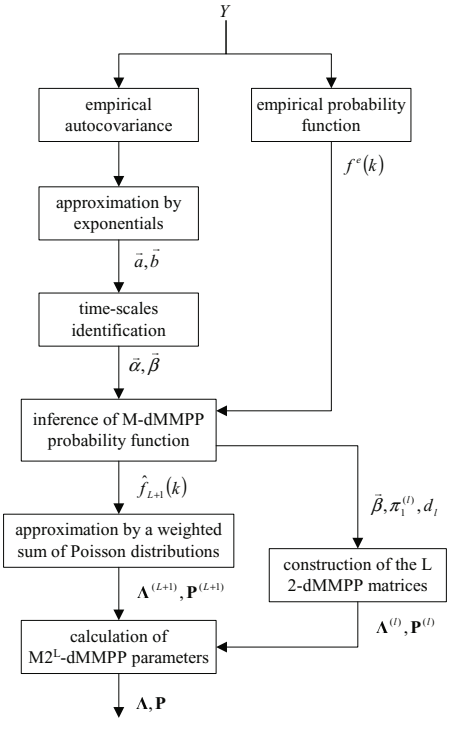

Fig. 3. Flow diagram of the inference procedure of the M2^L-MMPP model

decays that belong to the same traffic scale are aggregated in one component with the following parameters:

$$\alpha_l = \sum_{k=i_l}^{i_{l+1}-1} a_k \qquad \text{and} \qquad \beta_l = -\frac{\sum_{k=i_l}^{i_{l+1}-1} a_k b_k}{\alpha_l}. \tag{20}$$

where b_{i_l} and $b_{i_{l+1}-1}$ correspond to the first and last decay of the time scale. These parameters are used to fit the autocovariance function of the 2-dMMPP $Y^{(l)}$, since

$$\alpha_l = d_l^2 \pi_1^{(l)} \pi_2^{(l)} \qquad \text{and} \qquad \beta_l = c_l \tag{21}$$

where $\pi_i^{(l)}, i = 1, 2$ corresponds to the steady-state probabilities of $Y^{(l)}$, $d_l = |\lambda_2^{(l)} - \lambda_1^{(l)}|$ and $\beta_l = ln(1 - p_1^{(l)}2 - p_2^{(l)}1$, i.e., the fitted autocovariance function of $Y_1 + Y_2 + \ldots + Y_L$ is

$$\sum_{l=1}^{L} \alpha_l e^{k\beta_l}, \quad k = 1, 2, \ldots. \tag{22}$$

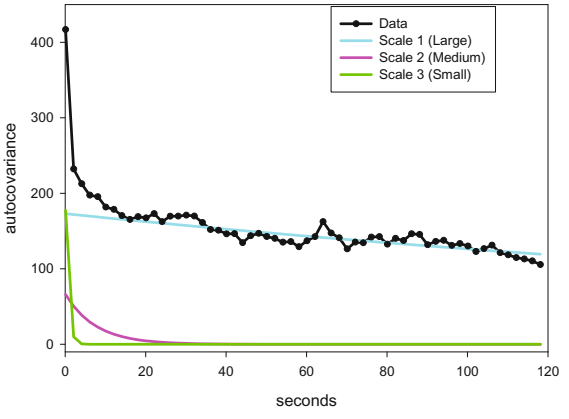

Fig. 4. Approximation of the autocovariance function

B. Inference of the M-dMMPP probability function and of the L 2-dMMPP parameters

The relation between the probability functions of the 2-dMMPPs, the M-dMMPP and the M2^L-dMMPP is defined by (17). In order to simplify the deconvolution of $f_{L+1}(k)$ and $f_l(k), l = 1, ..., L$, we consider that the Poisson arrival rate is zero in one state of each 2-dMMPP source; that is, $\lambda_1^{(l)} = 0$ and $\lambda_2^{(l)} = d_l$, for $l = 1, ..., L$. From (21), it follows that $d_l = \sqrt{\frac{\alpha_l}{\pi_1^{(l)}\pi_2^{(l)}}}, \quad l = 1, 2, \ldots, L$. The probability function of the M-dMMPP, f_{L+1}, is fitted jointly with the parameters $\pi_1^{(l)}$, $l = 1, ..., L$, through the following constrained minimization process:

$$\min_{\{\pi_1^{(l)},\, l=1,\ldots,L\},\{f_{L+1}(k),\, k=0,1,\ldots\}} \sum_k |o^e(k)| \tag{23}$$

where

$$o^e(k) = f^e(k) - \left(\hat{f}_1 \oplus ... \oplus \hat{f}_L \oplus f_{L+1}\right)(k) \tag{24}$$

subject to (21) and

$$0 < \pi_1^{(l)} < 1,\ l = 1, 2, \ldots, L, \quad f_{L+1}(k) > 0,\ k = 0, 1, \ldots, \quad \text{and} \quad \sum_{k=0}^{+\infty} f_{L+1}(k) = 1. \tag{25}$$

with f^e denoting the empirical probability function of the data. We denote by $\hat{f}_{L+1}$ the fitted probability function of the M-dMMPP. Note that $\pi_1^{(l)}$ is not allowed to be 0 or 1 because, in both cases, the l^{th} 2-dMMPP would degenerate into a Poisson process. The constrained minimization process given by (23)–(25) is a non-linear programming problem and in general, it is computationally demanding to obtain the global optimal solution. Accordingly, to solve this problem we consider two approximations: (i) we make $\pi_1^{(l)} = \pi_1^{(l+1)}, l = 1, \ldots, L-1$ and (ii) restrict the range of possible $\pi_1^{(l)}$ solutions

to be discrete and such that $\pi_1^{(l)} = 0.001k$, $k = 1, \ldots, 999$. Then a search process is used to find the minimum value of the objective function.

At this point all parameters of the 2-dMMPPs, $Y^{(1)}$, $Y^{(2)}$, $\ldots$, $Y^{(L)}$, have been determined and their corresponding 2-dMMPP matrices can be constructed in the following way:

$$\mathbf{P}^{(l)} = \begin{bmatrix} 1 - \pi_2^{(l)}(1 - e^{\beta_l}) & \pi_2^{(l)}(1 - e^{\beta_l}) \\ \pi_1^{(l)}(1 - e^{\beta_l}) & 1 - \pi_1^{(l)}(1 - e^{\beta_l}) \end{bmatrix} \tag{26}$$

$$\Lambda^{(l)} = \begin{bmatrix} 0 & 0 \\ 0 & d_l \end{bmatrix} \tag{27}$$

C. Inference of the M-dMMPP parameters

The next step is the inference of the number of states and Poisson arrival rates of the M-dMMPP from $\hat{f}_{L+1}$. To do this, we infer $\hat{f}_{L+1}$ as a weighted sum of Poisson probability functions, i.e., as the probability function of a finite Poisson mixture with an unknown number of components. The matching is carried out through an algorithm that progressively subtracts a Poisson probability function from $\hat{f}_{L+1}$, which is described in the flowchart of Figure 5. We represent the i^{th} Poisson probability function, with mean φ_i, by $g_{\varphi_i}(k)$. We define $h^{(i)}(k)$ as the difference between $\hat{f}_{L+1}(k)$ and the weighted sum of Poisson probability functions at the i^{th} iteration. Initially, we set $h^{(1)}(k) = \hat{f}_{L+1}(k)$. In each step, we first detect the maximum of $h^{(i)}(k)$. The corresponding k-value, $\varphi_i = [h^{(i)}]^{-1}\left(\max h^{(i)}(k)\right)$, will be considered the i^{th} Poisson rate of the M-dMMPP. We then calculate the weights of each Poisson probability function, $\boldsymbol{w}_i = [w_{1i}, w_{2i}, ..., w_{ii}]$, through the following set of linear equations:

$$\hat{f}_{L+1}(\varphi_l) = \sum_{j=1}^{i} w_{ji} g_{\varphi_j}(\varphi_l), \qquad l = 1, ..., i. \tag{28}$$

This assures that the fitting between $\hat{f}_{L+1}(k)$ and the weighted sum of Poisson probability functions is exact at φ_l points, for $l = 1, 2, \ldots, i$. The final step in each iteration is the calculation of the new difference function

$$h^{(i)}(k) = \hat{f}_{L+1}(k) - \sum_{j=1}^{i} w_{ji} g_{\varphi_j}(k). \tag{29}$$

The algorithm stops when the maximum of $h^{(i)}(k)$ is lower than a pre-defined percentage of the maximum of $\hat{f}_{L+1}(k)$ and M is made equal to i. After M has been determined, the parameters of the M-dMMPP, $\{(\pi_j^{(L+1)}, \lambda_j^{(L+1)}), j = 1, 2, \ldots, M\}$, are then set equal to

$$\pi_j^{(L+1)} = w_{jM} \qquad \text{and} \qquad \lambda_j^{(L+1)} = \varphi_j. \tag{30}$$

D. M2^L-dMMPP model construction

Finally, the M2^L-dMMPP process can be constructed using equations (7) and (8), where $\Lambda^{(L+1)}$, $\mathbf{P}^{(L+1)}$,$\Lambda^{(i)}$ and $\mathbf{P}^{(i)}$, $i = 1, ..., L$, were calculated in the last two steps.

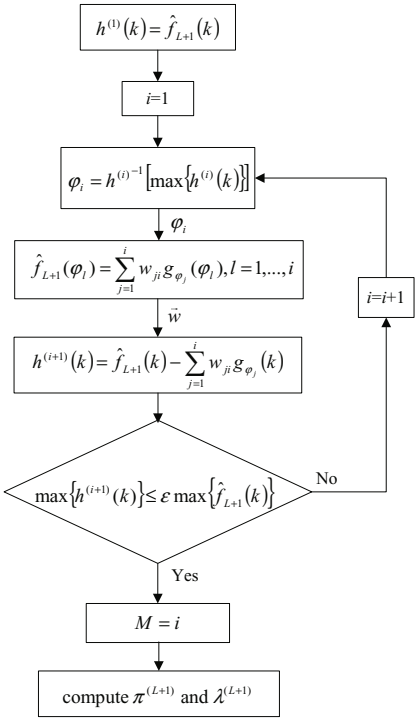

Fig. 5. Algorithm for calculation of the number of states and Poisson arrival rates of the M-dMMPP

4.1 Efficency Results

In [18] the efficiency of this fitting procedure was evaluated by applying it to trace UA, a trace of IP traffic measured at University of Aveiro (UA) that is representative of Internet access traffic produced within a University campus environment. The UA trace was measured on July 10^{th}, 2001, between 10.15am and 3.08pm, and comprises 20 millions packets with a mean rate of 1138 packets/s and a mean packet size of 557 bytes. This trace exhibits LRD behavior, which was confirmed by applying the method described in [27] (Figure 7). The sampling interval of the counting process was considered as 0.1 seconds, so octave j corresponds to 0.1×2^j seconds.

The performance of this fitting procedure (and all the others that will be described in the next sections) was evaluated using several evaluation criteria: (i) comparing both the probability and autocovariance functions of the packet arrival counts obtained with the fitted dMMPPs (theoretical) and with the original data traces; (ii) analyzing queuing behavior by comparing the PLR obtained, through trace-driven simulation, with the original data traces and simulated traces generated from the fitted dMMPPs (Figure 6). The results of trace driven simulation for the fitted traces were based on 10 replicas.

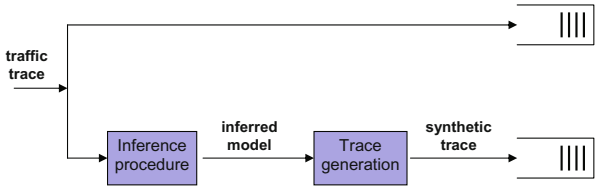

Fig. 6. Methodology for testing queueing behavior

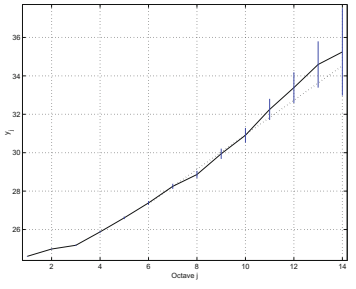

Fig. 7. Scaling analysis, UA

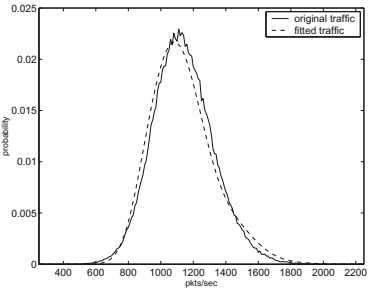

Fig. 8. Probability function, UA

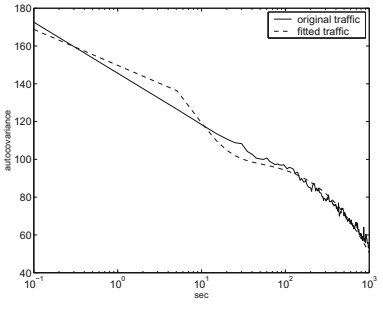

Fig. 9. Autocovariance function, UA

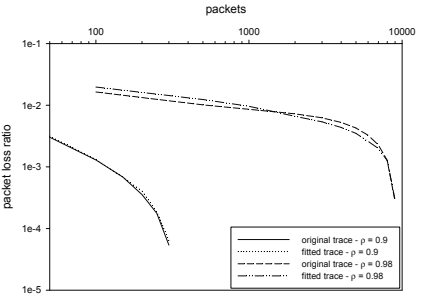

Fig. 10. Packet loss ratio versus buffer size, UA

The empirical autocovariance function was fitted by two exponentials with parameters $\boldsymbol{\alpha} = [1.00 \times 10^2 \; 6.87 \times 10^1]$ and $\boldsymbol{\beta} = [-6.91 \times 10^{-5} \; -1.28 \times 10^{-2}]$. With a resulting 12-states dMMPP, the fitting of the probability and autocovariance functions is very good (Figures 8 and 9, respectively), which reveals itself sufficient to get a very close matching of the PLR curve (Figure 10). The considered service rates are 685 KBytes/s and 629 KBytes/s, corresponding to link utilizations of $\rho = 0.9$ and $\rho = 0.98$, respectively. Both the original and the fitted traces exhibit LRD, with estimated Hurst parameters of $\widehat{H} = 0.952$ and $\widehat{H} = 0.935$, respectively.

5 Distributional Self-similar Models

This section proposes two traffic models, based on dMMPPs, designed to capture self-similar behavior over multiple time scales by fitting the empirical distribution of packet counts at each time scale. The number of time scales, L, is fixed *a priori* and the time scales are numbered in an increasing way, from $l = 1$ (corresponding to the largest time scale) to $l = L$ (corresponding to the smallest time scale).

5.1 Superposition Model

This model was firstly proposed in [19] and is based on the superposition of dMMPPs, where each dMMPP represents a specific time scale. Figure 11 illustrates the construction methodology of the dMMPP for the simple case of three time scales and two-state dMMPPs in each time scale. The dMMPP associated with time scale l is denoted by dMMPP$^{(l)}$ and the corresponding number of states by $N_{(l)}$. The flowchart of the inference procedure is represented in Figure 12 where, basically, the following three steps can be identified.

A. Computation of the data vectors (corresponding to the average number of arrivals per time interval) at each time scale
Having defined the time interval at the smallest time scale, Δt, the number of time scales, L, and the level of aggregation, a, the aggregation process starts by computing the data sequence corresponding to the average number of arrivals in the smallest time scale, $D^{(L)}(k), k = 1, 2, \ldots, N$. Then, it calculates the data sequences of the remaining time scales, $D^{(l)}(k), l = L-1, ..., 1$, corresponding to the average number of arrivals in intervals of length $\Delta t a^{(L-l)}$. This is given by

$$D^{(l)}(k) = \begin{cases} \Psi\left(\frac{1}{a}\sum_{i=0}^{a-1} D^{(l+1)}(k + ia^{L-l-1})\right), & \frac{k-1}{a^{L-l}} \in \mathbb{N}_0 \\ D^{(l)}(k-1), & \frac{k-1}{a^{L-l}} \notin \mathbb{N}_0 \end{cases} \tag{31}$$

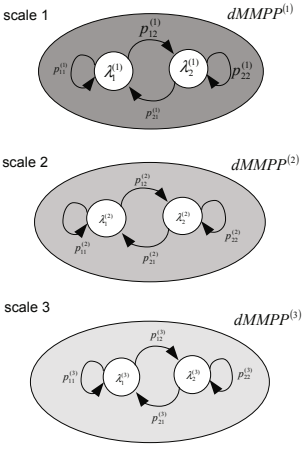

Fig. 11. Construction methodology of the superposition dMMPP model

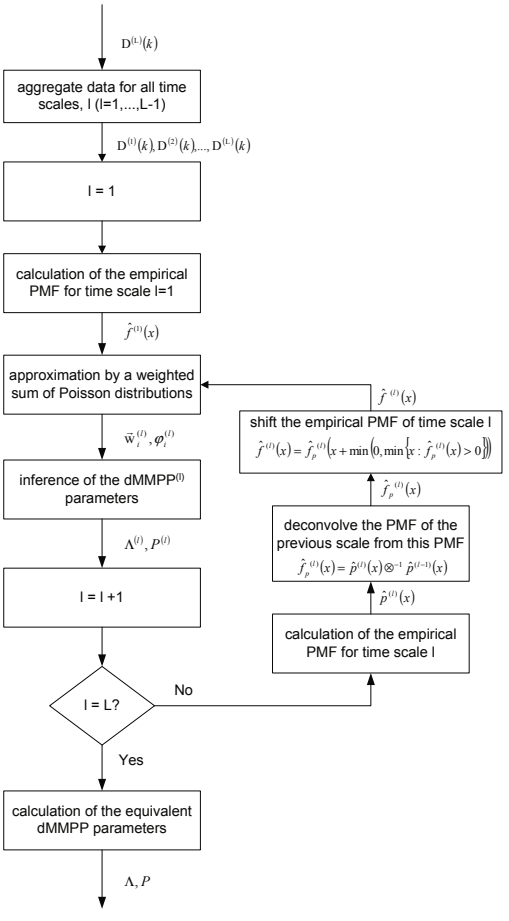

Fig. 12. Flow diagram of the inference procedure of the superposition model

where $\Psi(x)$ represents round toward the integer nearest x. Note that all data sequences have the same length N and that $D^{(l)}(k)$ is formed by sub-sequences of a^{L-l} successive equal values; these sub-sequences will be called *l-sequences*. The empirical distribution of $D^{(l)}(k)$ will be denoted by $\hat{p}^{(l)}(x)$.

Figure 13 illustrates the aggregation process for the particular case of considering only three time scales and an aggregation level of $a = 2$. The top part of the picture corresponds to the finest time scale (scale 3) and represents the number of arrivals per sampling interval. At time scale 2, the Figure represents the average number of arrivals per time interval of length $2\Delta t$, while at time scale 1 it represents the average number of arrivals per time interval of length $4\Delta t$, since the aggregation level is equal to 2.

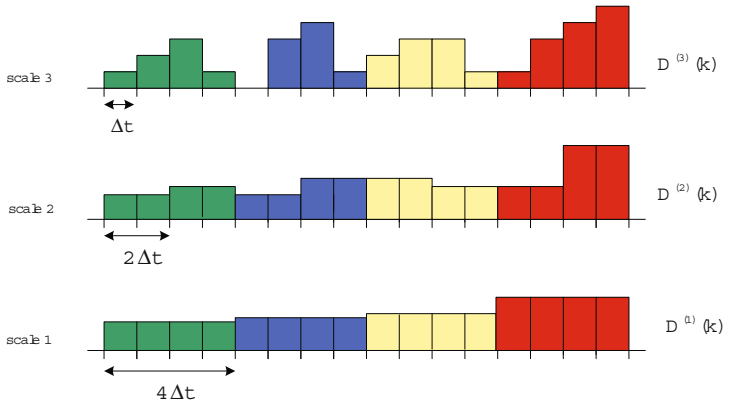

Fig. 13. Illustration of the aggregation process

B. For all time scales (going from the largest to the smallest one), calculation of the corresponding empirical PMF and inference of a dMMPP that matches the resulting PMF

Each dMMPP will be inferred from a PMF that represents its contribution to a particular time scale. For the largest time scale, this PMF is simply the empirical one. The traffic components due to time scale l, $l = 2, ..., L$, are obtained through deconvolution of the empirical PMFs of this and the previous time scales, i.e., $\hat{f}_p^{(l)}(x) = [\hat{p}^{(l)} \otimes^{-1} \hat{p}^{(l-1)}](x)$. However, this may result in probability mass at negative arrival rates for the dMMPP$^{(l)}$, which will occur whenever $\min\left\{x : \hat{p}^{(l-1)}(x) > 0\right\} < \min\left\{x : \hat{p}^{(l)}(x) > 0\right\}$. To correct these results, the dMMPP$^{(l)}$ will be fitted to

$$\hat{f}^{(l)}(x) = \hat{f}_p^{(l)}(x + e^{(l)}) \tag{32}$$

where $e^{(l)} = \min\left(0, \min\left\{x : \hat{f}_p^{(l)}(x) > 0\right\}\right)$, which assures $\hat{f}^{(l)}(x) = 0$, $x < 0$. The additional factors that are now introduced will be removed in the final step of the inference procedure.

The number of states, $N_{(l)}$, and the parameters of the dMMPP$^{(l)}$, $\{(\pi_j^{(1)}, \lambda_j^{(1)}), j = 1, 2, \ldots, N_{(1)}\}$, that adjusts the empirical PMF $\hat{f}^{(l)}(x)$ are calculated using the same procedure described in step 3 of the M2^L-dMMPP inference procedure.

The next step consists of associating one of the dMMPP$^{(l)}$ states with each time interval of the arriving process. Recall that the data sequences aggregated at time scale l have a^{L-l} successive equal values called l-sequences. The state assignment process considers only the first time interval of each l-sequence, defined by $i = a^{L-l}(k-1) + 1, k \in I\!N, i \in E^{(l)}$, where $E^{(l)}$ represents the set of time intervals associated with dMMPP$^{(l)}$. The state that is assigned to l-sequence i is calculated randomly according to the probability vector $\boldsymbol{\theta}^{(l)}(i) = \left\{\theta_1^{(l)}(i), \ldots, \theta_{N_{(l)}}^{(l)}(i)\right\}$, with

$$\theta_n^{(l)}(i) = \frac{g_{\lambda_n^{(l)}}\left(D^{(l)}(i)\right)}{\sum_{j=1}^{N_{(l)}} g_{\lambda_j^{(l)}}\left(D^{(l)}(i)\right)} \tag{33}$$

for $n = 1, ..., N_{(l)}$, where $\lambda_j^{(l)}$ represents the Poisson arrival rate of the j^{th} state of dMMPP$^{(l)}$, and $g_\lambda(y)$ represents a Poisson probability distribution function with mean λ. The elements of this vector represent the probability that the state j had originated the number of arrivals $D^{(l)}(k)$ at time interval k from time scale l.

After this step, we infer the dMMPP$^{(l)}$ transition probabilities, $p_{od}^{(l)}$, with $o, d = 1, ..., N_{(l)}$, by counting the number of transitions between each pair of states. If $n_{od}^{(l)}$ represents the number of transitions from state o to state d of the dMPPP$^{(l)}$, then

$$p_{od}^{(l)} = \frac{n_{od}^{(l)}}{\sum_{m=1}^{N_{(l)}} n_{om}^{(l)}}, o, d = 1, ..., N_{(l)} \tag{34}$$

The transition probability and the Poisson arrival rate matrices of the dMMPP$^{(l)}$ are then given by

$$\mathbf{P}^{(l)} = \begin{bmatrix} p_{11}^{(l)} & p_{12}^{(l)} & \cdots & p_{1N_{(l)}}^{(l)} \\ p_{21}^{(l)} & p_{22}^{(l)} & \cdots & p_{2N_{(l)}}^{(l)} \\ \cdots & \cdots & \cdots & \cdots \\ p_{N_{(l)}1}^{(l)} & p_{N_{(l)}2}^{(l)} & \cdots & p_{N_{(l)}N_{(l)}}^{(l)} \end{bmatrix} \tag{35}$$

$$\Lambda^{(l)} = \begin{bmatrix} \lambda_1^{(l)} & 0 & \dots & 0 \\ 0 & \lambda_2^{(l)} & \dots & 0 \\ \dots & \dots & \dots & \dots \\ 0 & 0 & \dots & \lambda_{N_{(l)}}^{(l)} \end{bmatrix} + e^{(l)}\mathbf{I} \tag{36}$$

The diagonal matrix of the steady-state probabilities is designated by $\Pi^{(l)}$.

Figure 14 schematically illustrates the main steps of the construction process for the superposition model, considering only the first two time scales. As was previously said, the empirical PMF corresponding to the largest time scale (scale 1) is estimated and the dMMPP that best adjusts it is inferred. For the next immediate scale (scale 2), the empirical PMF is estimated and then it is deconvolved from the PMF corresponding to time scale 1. The dMMPP that describes the contribution of time scale 2 for the arrival process is calculated based on the PMF that results from this deconvolution operation.

C. Calculation of the final dMMPP through the superposition of the dMMPPs inferred for each time scale

The equivalent dMMPP process is constructed using equations (7) and (8), where matrices $\mathbf{P}^{(l)}$ and $\Lambda^{(l)}$, $l = 1, ..., L$, were calculated in the last subsection. Besides, the additional factors introduced in 32 must be removed. Thus, the final $\Lambda^{(l)}$ will be given by

$$\Lambda = \Lambda - \sum_{l=2}^{L} e^{(l)} \cdot \mathbf{I} \tag{37}$$

where $\mathbf{I}$ is the identity matrix.

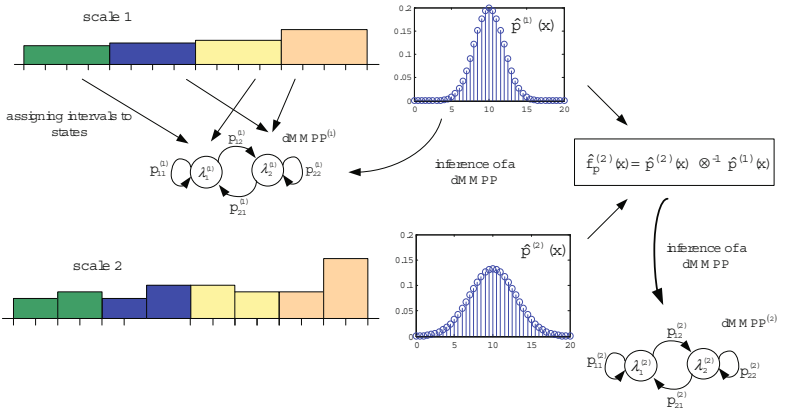

Fig. 14. Procedure for calculating the empirical PMFs and inferring the partial dMMPPs of the superposition model

5.2 Hierarchical Model

This model was firstly presented in [21] and is constructed using an hierarchical procedure, that successively decomposes dMMPP states into new dMMPPs, thus refining the traffic process by incorporating the characteristics offered by finer time scales (Figure 15). The procedure starts at the largest time scale by inferring a dMMPP that matches the empirical PMF corresponding to this time scale. As part of the parameter fitting procedure, each time interval of the data sequence is assigned to a dMMPP state; in this way, a new PMF can be associated with each dMMPP state. At the next finer time scale, each dMMPP state is decomposed into a new dMMPP that matches the contribution of this time scale to the PMF of the state it descends from. In this way, a child dMMPP gives a more detailed description of its parent state PMF. This refinement process is iterated until a pre-defined number of time scales is integrated. Finally, a dMMPP incorporating this hierarchical structure is derived.

The construction process of the hierarchical model can be described through a tree where, except for the root node, each tree node corresponds to a dMMPP state and each tree level to a time scale. A dMMPP state will be represented by a vector indicating the path in the tree from its higher level ancestor (i.e. the state it descends from at the largest scale, $l = 1$) to itself. Thus, a state at time scale l will be represented by some vector $\boldsymbol{s} = (s_1, s_2, ..., s_l)$, $s_i \in I\!N$. Each dMMPP will be represented by the state that generated it (i.e. its parent state), that is, dMMPP$^{\boldsymbol{s}}$ will represent the dMMPP generated by state $\boldsymbol{s}$. The root node of the tree corresponds to a virtual state, denoted by $\boldsymbol{s} = \emptyset$, that is used to represent the dMMPP of the largest time scale, $l = 1$. This dMMPP will be called the root dMMPP. Thus, the dMMPP states in the tree are characterized by $\boldsymbol{s} = (s_1, s_2, ..., s_l)$, $l \in I\!N$, with $s_{i+1} \in \{1, 2, \ldots, N_{\boldsymbol{s}_i}\}$, $i = 0, 1, \ldots, l-1$; here, $\boldsymbol{s}_{j]}$ denotes the sub-vector of $\boldsymbol{s}$ given by $(s_1, s_2, ..., s_j)$, with $j < |\boldsymbol{s}|$, and $\boldsymbol{s}_{0]} = \emptyset$, where $|\boldsymbol{s}|$ denotes the length of vector $\boldsymbol{s}$. Note that, using this notation, a vector $\boldsymbol{s}$ can either represent state $\boldsymbol{s}$ or the dMMPP generated by $\boldsymbol{s}$. Besides, the time scale of dMMPP$^{\boldsymbol{s}}$ is $|\boldsymbol{s}| + 1$.

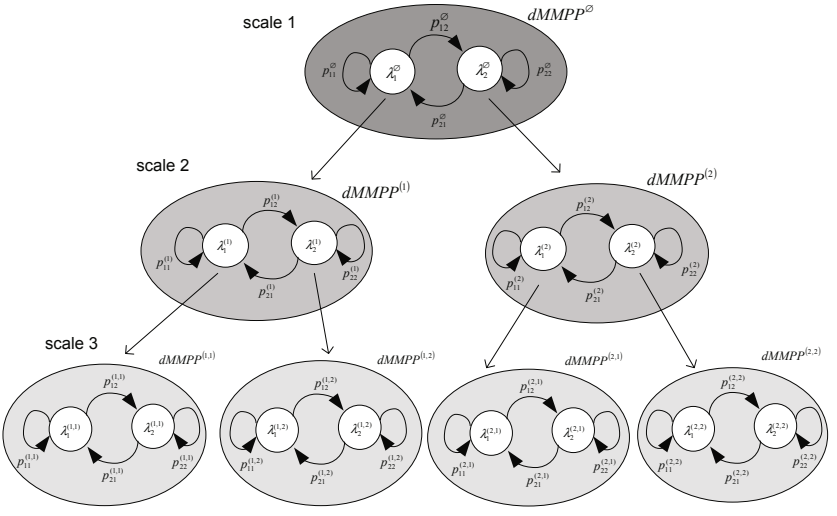

Fig. 15. Construction methodology of the hierarchical dMMPP model

Finally, let $E^{\boldsymbol{s}}$ denote the set of time intervals associated with state $\boldsymbol{s}$, i.e., with dMMPP$^{\boldsymbol{s}}$. Using this notation, the set associated with dMMPP$^{\emptyset}$ will be $E^{\emptyset} = \{1, 2, ..., N\}$, where N is the number of time intervals at the smallest time scale. Starting from $E^{\emptyset}$, the sets $E^{\boldsymbol{s}}$ are successively partitioned at each time scale in a hierarchical fashion. Thus, if states $\boldsymbol{s}$ and $\boldsymbol{t}$ are such that $|\boldsymbol{s}| = |\boldsymbol{t}| = l$ and $\boldsymbol{s} \neq \boldsymbol{t}$, then $E^{\boldsymbol{s}} \cap E^{\boldsymbol{t}} = \emptyset$ and $\bigcup_{\boldsymbol{s}:|\boldsymbol{s}|=l} E^{\boldsymbol{s}} = E^{\emptyset}$. Moreover, if state $\boldsymbol{s}$ is a parent of state $\boldsymbol{t}$, that is $\boldsymbol{t} = (\boldsymbol{s}, j)$, then $E^{\boldsymbol{t}} \subseteq E^{\boldsymbol{s}}$ and $\bigcup_{j=1,...,N_{\boldsymbol{s}}} E^{(\boldsymbol{s},j)} = E^{\boldsymbol{s}}$.

The inference procedure is represented schematically in the flowchart of Figure 16, where the following three main steps can be identified.

A. Computation of the data vectors (corresponding to the average number of arrivals per time interval) for each time scale

This step is equal to the one described for the superposition model.

B. For all time scales (going from the largest to the smallest one), calculation of the corresponding empirical PMF and inference of a dMMPP that matches the resulting PMF

Each dMMPP will be inferred from a PMF that represents its contribution to a particular time scale. For the largest time scale, this PMF is simply the empirical one, but for all other time scales l, $l = 2, ..., L$, the PMF represents the contribution of the time scale to the PMF of its parent state. The contribution of a dMMPP at time scale l generated from state $\boldsymbol{s}$ corresponds also to the deconvolution of empirical PMFs, but now calculated over the set of time intervals $E^{\boldsymbol{s}}$, at this time scale $l = |\boldsymbol{s}| + 1$ and the previous time scale $l - 1 = |\boldsymbol{s}|$, i.e., $\hat{f}_p^{\boldsymbol{s}}(x) = \left[\hat{p}^{\boldsymbol{s},|\boldsymbol{s}|+1} \otimes^{-1} \hat{p}^{\boldsymbol{s},|\boldsymbol{s}|}\right](x)$, where $\hat{p}^{\boldsymbol{s},l}$ represents the PMF obtained from the data sequence $D^l(k), k \in E^{\boldsymbol{s}}$. Note that the two empirical PMFs are obtained from the same set of time intervals but aggregated at

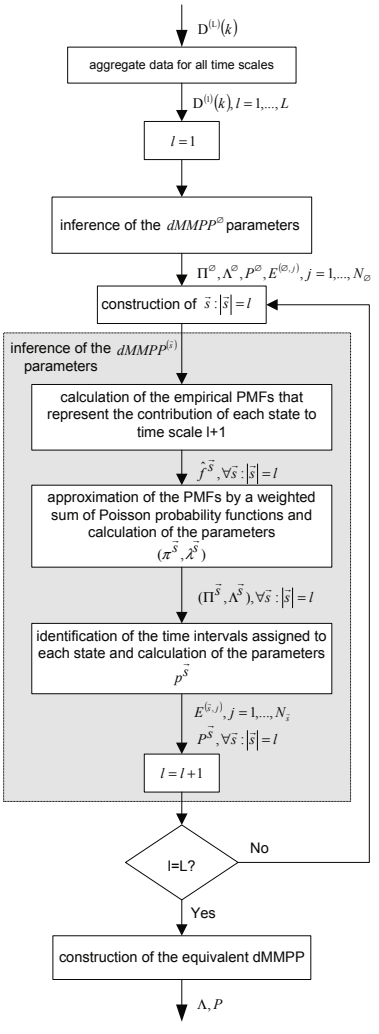

Fig. 16. Flow diagram of the inference procedure of the hierarchical model

different levels. Once again, these operations may result in probability mass at negative arrival rates for the dMMPP$^{\boldsymbol{s}}$, which will occur whenever $\min\left\{x : \hat{p}^{\boldsymbol{s},|\boldsymbol{s}|}(x) > 0\right\} < \min\left\{x : \hat{p}^{\boldsymbol{s},|\boldsymbol{s}|+1}(x) > 0\right\}$. These results must be corrected using equation 32, with (l) replaced by $\boldsymbol{s}$.

The number of states, $N_{\boldsymbol{s}}$, and the parameters of the dMMPP$^{\boldsymbol{s}}$, $\{(\pi_j^{\boldsymbol{s}}, \lambda_j^{\boldsymbol{s}}), j = 1, 2, \ldots, N_{\boldsymbol{s}}\}$, that adjusts the empirical PMF $\hat{f}^{\boldsymbol{s}}(x)$ are calculated using the same procedure described in step 3 of the M2^L-dMMPP inference procedure.

The next step consists of associating one of the dMMPP$^{\boldsymbol{s}}$ states with each time interval of the arriving process. The set of time intervals associated with dMMPP$^{\boldsymbol{s}}$ is $E^{\boldsymbol{s}}$ and the goal here is to partition $E^{\boldsymbol{s}}$ into subsets $E^{(\boldsymbol{s},j)}, j = 1, ..., N_{\boldsymbol{s}}$. Now, the state assignment process considers only the first time interval of each l-sequence, defined by

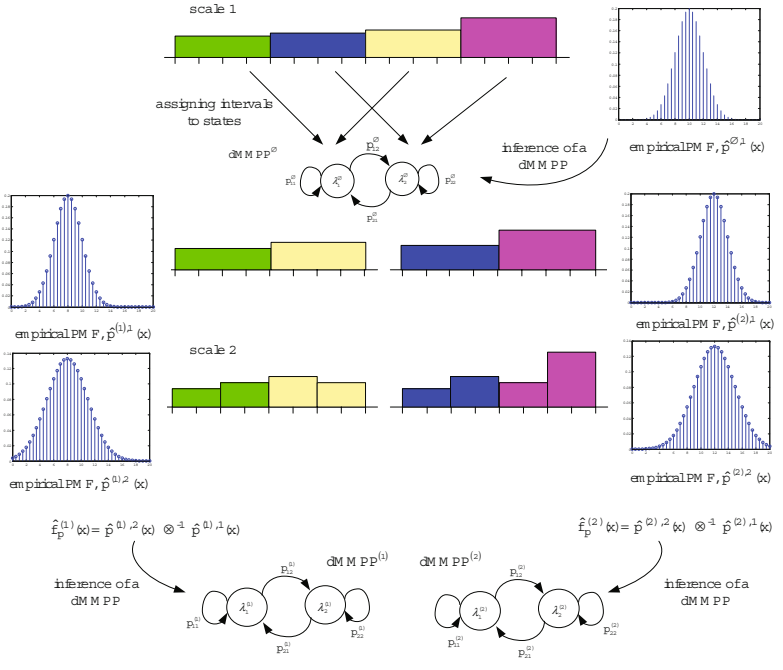

Fig. 17. Procedure for calculating the empirical PMFs and inferring the partial dMMPPs of the decomposition model

$i = a^{L-(|\boldsymbol{s}|+1)}(k-1)+1, k \in I\!N, i \in E^{\boldsymbol{s}}$. The state that is assigned to l-sequence i is calculated randomly according to the probability vector $\boldsymbol{\theta}^{\boldsymbol{s}}(i) = \left\{\theta_1^{\boldsymbol{s}}(i), \ldots, \theta_{N_{\boldsymbol{s}}}^{\boldsymbol{s}}(i)\right\}$, with

$$\theta_n^{\boldsymbol{s}}(i) = \frac{g_{\lambda_n^{\boldsymbol{s}}}\left(D^{|\boldsymbol{s}|+1}(i)\right)}{\sum_{j=1}^{N_{\boldsymbol{s}}} g_{\lambda_j^{\boldsymbol{s}}}\left(D^{|\boldsymbol{s}|+1}(i)\right)} \tag{38}$$

for $n = 1, ..., N_{\boldsymbol{s}}$.

The dMMPP$^{\boldsymbol{s}}$ transition probabilities, $p_{od}^{\boldsymbol{s}}$, $o, d = 1, ..., N_{\boldsymbol{s}}$, are calculated through equation 34 with (l) replaced by $\boldsymbol{s}$. In this way, the transition probability and the Poisson arrival rate matrices are also given by equations 35 and 36, respectively.

Figure 17 schematically illustrates the main steps of the construction process for the decomposition model, considering only the first two time scales. For the largest time scale (scale 1), the empirical PMF is estimated and the dMMPP that best adjusts it is inferred (dMMPP$^{\emptyset}$). Each time interval of the data sequence is then assigned to each dMMPP state and the next step consists on estimating the empirical PMFs associated to each state. For the next immediate scale (scale 2), the empirical PMFs associated to each state will also be estimated and then they are deconvolved from the PMFs corresponding to time scale 1 and to the same states. The dMMPPs that describe the contribution of time scale 2 for the arrival process are calculated based on the PMFs that result from these deconvolution operations.

C. Calculation of matrices Λ and $\mathbf{P}$ of the dMMPP that incorporates the hierarchical structure

In this step we have to construct a dMMPP equivalent to the tree structure of dMMPPs derived in previous steps. The goal is to incorporate in the model the level of detail given by the finer time scale, so the equivalent dMMPP will have a number of states equal to the number of states in smallest time scale of the tree structure, L. These can be identified by $\boldsymbol{s} = (s_1, s_2, ..., s_L)$; each state is associated with its ancestor states $\boldsymbol{s}_{i+1]} = (s_1, s_2, ..., s_{i+1})$, $i = 0, 1, \ldots, L-1$ of the dMMPP$^{\boldsymbol{s}_{i]}}$.

Thus, the states of the equivalent dMMPP will have Poisson rates which are the sum of the Poisson rates of its ancestors in the tree structure, i.e.,

$$\lambda_{\boldsymbol{s}} = \sum_{j=0}^{L-1} \lambda_{s_{j+1}}^{\boldsymbol{s}_{j]}} \tag{39}$$

The transition between each pair of states is determined by the shortest path in the tree structure, going through the root dMMPP, that joins the two states. Any pair of states descend from one or more common dMMPPs. The first one, at the time scale with higher l, will be denoted by $\boldsymbol{s} \wedge \boldsymbol{t} = (s_1, s_2, ..., s_k)$ where $k = \max\{i : s_j = t_j, j = 1, 2, ..., i\}$.

We first consider the case of $\boldsymbol{s} \neq \boldsymbol{t}$. The probability of transition from $\boldsymbol{s}$ to $\boldsymbol{t}$, $p_{\boldsymbol{s},\boldsymbol{t}}$, is given by the product of three factors. The first factor accounts for the time scales where $\boldsymbol{s}$ and $\boldsymbol{t}$ have the same associated states and is given by

$$\phi_{\boldsymbol{s},\boldsymbol{t}} = \begin{cases} \prod_{j=0}^{|\boldsymbol{s}\wedge\boldsymbol{t}|-1} p_{s_{j+1},s_{j+1}}^{\boldsymbol{s}_{j]}}, |\boldsymbol{s} \wedge \boldsymbol{t}| \neq 0 \\ 1, |\boldsymbol{s} \wedge \boldsymbol{t}| = 0 \end{cases} \tag{40}$$

The second factor accounts for the transition in the time scale where $\boldsymbol{s}$ and $\boldsymbol{t}$ are associated to different states of the same dMMPP, which corresponds to $p_{s_{|\boldsymbol{s}\wedge\boldsymbol{t}|+1},t_{|\boldsymbol{s}\wedge\boldsymbol{t}|+1}}^{\boldsymbol{s}\wedge\boldsymbol{t}}$. The third factor accounts for the steady-state probabilities of states associated to $\boldsymbol{t}$ in the time scales that are not common to $\boldsymbol{s}$ and is given by

$$\psi_{\boldsymbol{s},\boldsymbol{t}} = \prod_{j=|\boldsymbol{s}\wedge\boldsymbol{t}|+1}^{L-1} \pi_{t_{j+1}}^{\boldsymbol{t}_{j]}} \tag{41}$$

where an empty product is equal to one.
Finally, for $\boldsymbol{s} \neq \boldsymbol{t}$,

$$p_{\boldsymbol{s},\boldsymbol{t}} = \phi_{\boldsymbol{s},\boldsymbol{t}} p_{s_{|\boldsymbol{s}\wedge\boldsymbol{t}|+1},t_{\boldsymbol{s}\wedge\boldsymbol{t}+1}}^{\boldsymbol{s}\wedge\boldsymbol{t}} \psi_{\boldsymbol{s},\boldsymbol{t}} \tag{42}$$

In case $\boldsymbol{s} = \boldsymbol{t}$, it is simply

$$p_{\boldsymbol{s},\boldsymbol{t}} = \phi_{\boldsymbol{s},\boldsymbol{t}} \tag{43}$$

5.3 Efficiency Results

These fitting procedures were applied to the Kazaa trace, a trace measured at the backbone of a Portuguese ISP network characterizing the downstream traffic from 10

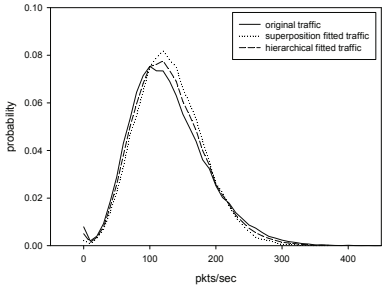

Fig. 18. PMF at the smallest time scale, Kazaa

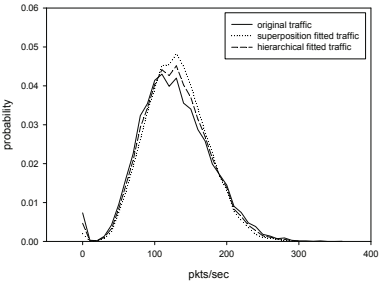

Fig. 19. PMF at the intermediate time scale, Kazaa

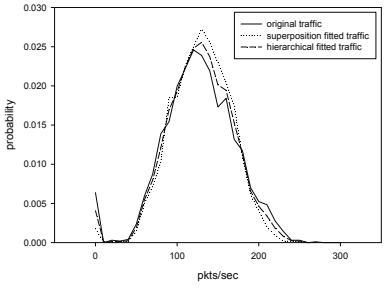

Fig. 20. PMF at the largest time scale, Kazaa

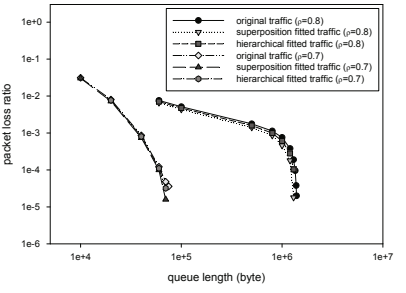

Fig. 21. Packet loss ratio versus buffer size, Kazaa

users of the file sharing application Kazaa. The Kazaa trace was measured on October 18^{th} 2001, between 10.26pm and 11.31pm, and comprises 1 million packets with a mean rate of 131140 packets/s and a mean packet size of 1029 bytes. This trace exhibits self-similar characteristics and three different time scales were considered: 0.1s, 0.2s and 0.4s. Larger aggregation levels were also considered, with good fitting results. Both fitting approaches were able to capture the traffic LRD behavior and the agreement between the PMFs corresponding to the original and dMMPP fitted traces, for the smallest, intermediate and largest time scales, was very good, as can be seen from figures 18, 19 and 20. These results were achieved with resulting dMMPPs having about 288 states in the superposition model and 38 states in the hierarchical model.

Considering queuing performance, Figure 21 shows that PLR behavior is very well approximated by the equivalent dMMPPs for both utilization ratios ($\rho = 0.7$ and $\rho = 0.8$). However, as the utilization ratio increases the deviation slightly increases, because the sensitivity of the metrics variation to a slight difference in the compared traces is higher. Thus, the proposed fitting approaches provide a close match of the PMFs at each time scale and this agreement reveals itself sufficient to drive a good queuing performance in terms of packet loss ratio.

The computational complexity of both fitting methods is small. This complexity, as well as the number of states of the resulting dMMPPs, is directly related to the level of accuracy used to approximate the empirical PMFs at each time scale by weighted

sums of Poisson probability functions. The performance of both inference procedures is very similar. Thus, it is not easy to recommend one of approaches over the other based solely on their associated performances. One argument that clearly favors the hierarchical approach is that the numbers of states of the resulting dMMPPs are smaller than the corresponding numbers for the superposition approach. This may be due to the fact that in the hierarchical approach and as the time scale increases, dMMPPs are fitted to successively smaller sets of intervals whose arrivals characteristics tend to increase in homogeneity and, thus, tend to have associated a smaller number of states than the dMMPP fitted through the superposition approach for the same time scale. However, the contribution of each time scale for the characterization of the aggregate traffic characteristics is interpreted in an easier and more natural way through the superposition approach. Note also that, for the same number of states, a smaller number of dMMPPs and corresponding parameters tend to be needed to compute the final dMMPP using the superposition approach than using the hierarchical approach.

6 Joint Characterization of Packet Arrivals and Packet Sizes - dBMAP

The dBMAP jointly characterizes the packet arrival process and the packet size distribution, being able to achieve an accurate prediction of the queuing behavior for IP traffic exhibiting LRD behavior. In this process, that was firstly presented in [30], packet arrivals occur according to a dMMPP (that can be any one of the previously described models) and each arrival is further characterized by a packet size with a general distribution that may depend on the phase of the dMMPP (Figure 22). This construction process allows having a packet size distribution closely related to the packet arrival process, and is in contrast with the approach followed by [22] where the packet size distribution is fitted prior to the matching of the packet arrival rates.

Lets consider that the packets have independent sizes, with the size of packets arriving in phase i having probability function $q_i = \{q_i(n),\ n \in \mathbb{N}\}$. If we let (X, J)

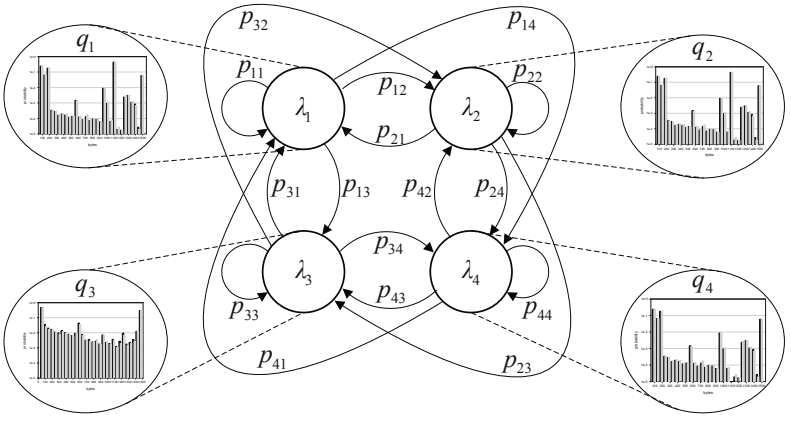

Fig. 22. Construction methodology of the BMAP model

denote the dMMPP, on the state space $\mathbb{N}_0 \times S$ and having parametrization $(\mathbf{P}, \Lambda)$, that models the packet arrival process, then the byte arrival process (Y, J) is a dBMAP, on the state space $\mathbb{N}_0 \times S$, satisfying equation 4 with

$$q_{ij}(n) = \sum_{l=0}^{+\infty} e^{-\lambda_j} \frac{\lambda_j^l}{l!} q_j^{(l)}(n) \tag{44}$$

for $i, j \in S$ and $n \in \mathbb{N}_0$, where $q_j^{(l)}$ denotes de convolution of order l of q_j. Thus, (Y, J) is a dBMAP on the state space $\mathbb{N}_0 \times S$, such that, for $n, m \in \mathbb{N}_0$,

$$P(Y_{k+1} = m + n,\, J_{k+1} = j | Y_k = m,\, J_k = i) = p_{ij} \sum_{l=0}^{+\infty} e^{-\lambda_j} \frac{\lambda_j^l}{l!} q_j^{(l)}(n) \tag{45}$$

which we express by saying that (Y, J) has *type-II parametrization* $(\mathbf{P}, \Lambda, \{q_i,\, i \in S\})$. S is the phase set of the (Y, J) dBMAP.

The packet size characterization is carried out in an independent way for each state of the inferred dMMPP and involves two steps: (i) association of each time slot to one of the dMMPP states and (ii) inference of a packet size distribution for each state of the dMMPP. In the first step, we scan all time slots of the empirical data. A time slot in which k packet arrivals were observed is randomly assigned to a state, according to the probability vector $\boldsymbol{\theta}(k) = \{\theta_1(k), \ldots, \theta_{N_B}(k)\}$, where $\theta_i(k)$ represents the probability that the observed k packet arrivals were originated in state i and N_B is the number of states of the dMMPP. This is given by

$$\theta_i(k) = \frac{\pi_i\, g_{\lambda_i}(k)}{\sum_{j=1}^{N_B} \pi_j\, g_{\lambda_j}(k)} \tag{46}$$

where λ_j represents the Poisson packet arrival rate of the dMMPP and π_j the corresponding steady-state probability (as stated before, $g_\lambda(y)$ represents a Poisson probability distribution function with mean λ).

The inference of the packet size distribution in each state resorts to histograms. The inference of each histogram uses only the packets that arrived during the time slots previously associated with the state for which we are inferring the packet size distribution. Note that some low-probability states may have no packets associated with them, making impossible the packet characterization specifically for these states. We associate a packet size distribution to these states that considers all data packets, i.e., the packet size distribution unconditioned on the dMMPP states. The histograms result in the packet size distributions $q_i = \{q_i(n),\, n \in \mathbb{N}\}$, for $i = 1, 2, ..., N_B$.

6.1 Efficiency Results

Reference [30] evaluated the efficiency of a dBMAP where the packet arrival process was modelled using the M2^L-dMMPP described in section 4 and the packet size process was modelled using the procedure described in section 6. The UA trace was also used to assess the efficiency of this traffic model, so the results of applying the M2^L-dMMPP

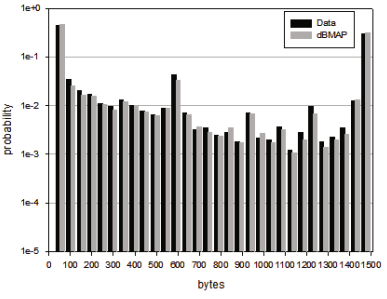

Fig. 23. Packet size distribution, UA

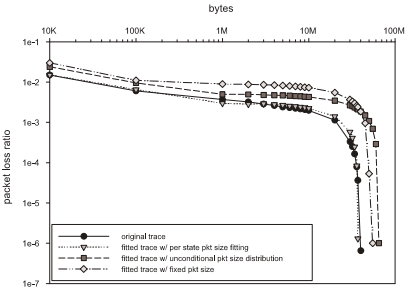

Fig. 24. Packet loss ratio versus buffer size, UA

fitting procedure to the packet arrival process were already presented in section 4. The packet size distribution is essentially bimodal with two pronounced peaks around 40 and 1500 bytes, presenting also non negligible values at 576 and 885 bytes. There was an excellent agreement between the original and fitted packet size distributions (Figure23), leading to a good match between the original and fitted distributions of the bytes/s processes.

For the dBMAP, four types of input traffic are considered in the trace-driven simulation: (i) the original trace, (ii) a trace generated according to the fitted dBMAP, (iii) a trace where the arrival instants were generated according to the fitted dMMPP arrival process and the packet size according to the unconditional packet size distribution of the fitted dBMAP and (iv) a trace where the arrival instants were also generated according to the fitted dMMPP arrival process but the packet size is fixed and equal to the average packet size of the original trace. In order to analyze queuing behavior, we considered a queue with a service rate of 700 Kbytes/s, corresponding to a link utilization of $\rho = 0.90$, and varied the buffer size from 10 Kbytes to 60 Mbytes. As it can be observed in Figure 24, there is a close agreement between the curves corresponding to the original trace and to the trace generated according to the fitted 12-dBMAP, for all buffer size values. In contrast, for the other two curves corresponding to traces where the packet size is fitted independently of the packet arrival process, significant deviations are obtained. Thus, detailed modeling of the packet size and of the correlations with the packet arrivals is clearly required.

7 Conclusion

Accurate modeling of certain types of IP traffic involves the description of the packet arrival process and the packet size distribution. This tutorial discussed the suitability of Markovian models to describe traffic that exhibits self-similarity and long range dependence behaviours. Three traffic models, based on MMPPs, were designed to describe the packet arrival process by capturing the self-similar behavior over multiple time scales: the first model is based on a parameter fitting procedure that matches both the autocovariance and marginal distribution of the counting process and the

MMPP is constructed as a superposition of L two-state MMPPs, designed to match the autocovariance function, and one M-MMPP designed to match the marginal distribution. The second model is a superposition of MMPPs, where each MMPP describes a different time scale of the packet arrival process. The third model is obtained as the equivalent to an hierarchical construction process that, starting at the coarsest time scale, successively decomposes MMPP states into new MMPPs to incorporate the characteristics offered by finner time scales. For all three traffic models, the number of states is not fixed *a priori* but is determined as part of the inference procedure. In order to closely match not only the packet arrival process but also the packet size distribution a dBMAP was also presented and discussed: packet arrivals occur according to a dMMPP and each arrival is further characterized by a packet size with a general distribution that may depend on the phase of the dMMPP. This allows having a packet size distribution closely related to the packet arrival process. The accuracy of the proposed models was evaluated by comparing the probability mass function at each time scale, as well as the packet loss ratio corresponding to measured traces and to traces synthesized according to the proposed models. The accuracy analysis was based on traffic traces exhibiting LRD and self-similar behaviors.

References

1. Leland, W., Taqqu, M., Willinger, W., Wilson, D.: On the self-similar nature of Ethernet traffic (extended version). IEEE/ACM Transactions on Networking 2(1), 1–15 (1994)
2. Beran, J., Sherman, R., Taqqu, M., Willinger, W.: Long-range dependence in variable-bit rate video traffic. IEEE Transactions on Communications 43(2/3/4), 1566–1579 (1995)
3. Crovella, M., Bestavros, A.: Self-similarity in World Wide Web traffic: Evidence and possible causes. IEEE/ACM Transactions on Networking 5(6), 835–846 (1997)
4. Paxson, V., Floyd, S.: Wide-area traffic: The failure of Poisson modeling. IEEE/ACM Transactions on Networking 3(3), 226–244 (1995)
5. Ryu, B., Elwalid, A.: The importance of long-range dependence of VBR video traffic in ATM traffic engineering: Myths and realities. ACM Computer Communication Review 26, 3–14 (1996)
6. Grossglauser, M., Bolot, J.C.: On the relevance of long-range dependence in network traffic. IEEE/ACM Transactions on Networking 7(5), 629–640 (1999)
7. Nogueira, A., Valadas, R.: Analyzing the relevant time scales in a network of queues. In: Proceedings of SPIE's International Symposium ITCOM 2001 (August 2001)
8. Heyman, D., Lakshman, T.: What are the implications of long range dependence for VBR video traffic engineering? IEEE/ACM Transactions on Networking 4(3), 301–317 (1996)
9. Neidhardt, A., Wang, J.: The concept of relevant time scales and its application to queuing analysis of self-similar traffic. In: Proceedings of SIGMETRICS 1998/PERFORMANCE 1998, pp. 222–232 (1998)
10. Yoshihara, T., Kasahara, S., Takahashi, Y.: Practical time-scale fitting of self-similar traffic with Markov-modulated Poisson process. Telecommunication Systems 17(1-2), 185–211 (2001)
11. Salvador, P., Valadas, R.: Framework based on markov modulated poisson processes for modeling traffic with long-range dependence. In: van der Mei, R.D., de Bucs, F.H.S. (eds.) Internet Performance and Control of Network Systems II, August 2001. Proceedings SPIE, vol. 4523, pp. 221–232 (2001)

12. Salvador, P., Valadas, R.: A fitting procedure for Markov modulated Poisson processes with an adaptive number of states. In: Proceedings of the 9th IFIP Working Conference on Performance Modelling and Evaluation of ATM & IP Networks (June 2001)
13. Andersen, A., Nielsen, B.: A Markovian approach for modeling packet traffic with long-range dependence. IEEE Journal on Selected Areas in Communications 16(5), 719–732 (1998)
14. Hajek, B., He, L.: On variations of queue response for inputs with the same mean and autocorrelation function. IEEE/ACM Transactions on Networking 6(5), 588–598 (1998)
15. Feldmann, A., Gilbert, A., Willinger, W.: Data networks as cascades: Investigating the multifractal nature of internet WAN traffic. In: Proceedings of SIGCOMM, pp. 42–55 (1998)
16. Feldmann, A., Gilbert, A.C., Huang, P., Willinger, W.: Dynamics of IP traffic: A study of the role of variability and the impact of control. In: SIGCOMM, pp. 301–313 (1999)
17. Riedi, R., Véhel, J.: Multifractal properties of TCP traffic: a numerical study. Technical Report No 3129, INRIA Rocquencourt, France (February 1997), www.dsp.rice.edu/~riedi
18. Salvador, P., Valadas, R., Pacheco, A.: Multiscale fitting procedure using Markov modulated Poisson processes. Telecommunications Systems 23(1-2), 123–148 (2003)
19. Nogueira, A., Salvador, P., Valadas, R., Pacheco, A.: Fitting self-similar traffic by a superposition of mmpps modeling the distribution at multiple time scales. IEICE Transactions on Communications E84-B(8), 2134–2141 (2003)
20. Nogueira, A., Salvador, P., Valadas, R., Pacheco, A.: Modeling self-similar traffic through markov modulated poisson processes over multiple time scales. In: Proceedings of the 6th IEEE International Conference on High Speed Networks and Multimedia Communications (July 2003)
21. Nogueira, A., Salvador, P., Valadas, R., Pacheco, A.: Hierarchical approach based on mmpps for modeling self-similar traffic over multiple time scales. In: Proceedings of the First International Working Conference on Performance Modeling and Evaluation of Heterogeneuous Networks (HET-NETs 2003) (July 2003)
22. Klemm, A., Lindemann, C., Lohmann, M.: Traffic modeling of IP networks using the batch Markovian arrival process. Performance Evaluation 54(2), 149–173 (2003)
23. Gao, J., Rubin, I.: Multifractal analysis and modeling of long-range-dependent traffic. In: Proceedings of International Conference on Communications ICC 1999, June 1999, pp. 382–386 (1999)
24. Lucantoni, D.M.: New results on the single server queue with a batch Markovian arrival process. Stochastic Models 7(1), 1–46 (1991)
25. Lucantoni, D.M.: The BMAP/G/1 queue: A tutorial. In: Donatiello, L., Nelson, R. (eds.) Models and Techniques for Performance Evaluation of Computer and Communication Systems, pp. 330–358. Springer, Heidelberg (1993)
26. Pacheco, A., Prabhu, N.U.: Markov-additive processes of arrivals. In: Dshalalow, J.H. (ed.) Advances in Queueing: Theory and Methods, ch. 6, pp. 167–194. CRC, Boca Raton (1995)
27. Veitch, D., Abry, P.: A wavelet based joint estimator for the parameters of LRD. IEEE Transactions on Information Theory 45(3) (April 1999)
28. Feldmann, A., Whitt, W.: Fitting mixtures of exponentials to long-tail distributions to analyze network performance models. Performance Evaluation 31(3-4), 245–279 (1997)
29. Osborne, M., Smyth, G.: A modified prony algorithm for fitting sums of exponential functions. SIAM J. Sci. Statist. Comput. 16, 119–138 (1995)
30. Salvador, P., Pacheco, A., Valadas, R.: Modeling IP traffic: Joint characterization of packet arrivals and packet sizes using BMAPs. Computer Networks Journal 44, 335–352 (2004)